Pol. J. Environ. Stud. Vol. XX, No. X (XXXX), 1-12
DOI: *10.15244/pjoes/213365* ONLINE PUBLICATION DATE: 2025-12-10

Original Research

Phytomediated Synthesis of Iron Particles Using Dark Tea Extract for Catalytic Degradation of Malachite Green

Xiyao Liu, Wenchang Zhao, Yan Xie, Jie Gao, Xiaoyan Zheng, Xinyi Li, Yuling Lin, Xi Yao, Xinya Fu, Chenjie Liu, Lingyi Cai, Zishen Hu, Chenhang Yu, Tzu-Hsing Ko*

College of New Energy and Materials, Ningde Normal University, Ningde 352100, Fujian, China

Received: 21 May 2025
Accepted: 19 October 2025

Abstract

The synthesis and characterization of iron particles (Fe-Ps) derived from a reaction between dark tea extract and an iron precursor were investigated. FTIR and XRD analyses confirmed the interaction of iron with plant constituents and the amorphous nature of the Fe-Ps. The catalytic activity of the Fe-Ps sample on malachite green (MG) degradation in a Fenton system was evaluated, along with operational factors such as reaction time, Fe-Ps loading, MG concentration, and reusability. The experimental results showed a significant enhancement in degradation efficiency when H_2O_2 was combined with the synthesized Fe-Ps, compared to the individual use of H_2O_2. The degradation efficiency of MG by the synthesized Fe-Ps remained stable at 90% after five cycles, indicating good reusability. The decrease in degradation efficiency after the reusability process was attributed to several factors, including changes in the crystallite phase, the decrease in BET surface area, and the higher chloride content in the sample. The kinetic results demonstrated the suitability of the BMG model for describing the reaction between the synthesized Fe-Ps and MG in a Fenton system. The BMG model facilitated the determination of the superior reaction rate constant and degradation capacity. These findings provide valuable insights into the potential application of tea residues in the synthesis of metal particles.

Keywords: iron particles, dark tea extract, fenton system, reusability, BMG model

Introduction

Iron is a plentiful element that is distributed throughout the Earth's crust, comprising approximately 4.8% of the total weight of crustal elements and ranking as the second most abundant metal after aluminum. As a key transition metal, iron serves as the foundation of modern infrastructure, playing an indispensable role in construction, manufacturing, and industry worldwide. The predominant form of iron in nature is oxide. In addition to its well-known use in the production of steel and stainless steel, the application of iron and iron oxides is also widespread in catalysis, adsorption, sensor technology, magnetic data storage, and energy

*e-mail: hsingko@gmail.com
ORCID iD: 0000-0002-8824-6739

storage due to their exceptional optical, thermal, mechanical, and electrical properties [1-7]. There are three major methods for iron and its oxide fabrication, including chemical, physical, and biological methods. Chemical-based preparations constitute approximately 90% of iron and iron oxide synthesis due to their high yield. However, this method necessitates the use of a substantial quantity of chemical reagents, which has a deleterious effect on the environment. An alternative approach involves the utilization of biological-based technology for the synthesis of iron and oxides. The biologically based methods principally consist of protein-mediated, bacterial-mediated, fungal-mediated, and plant-mediated technologies, accounting for 66%, 21%, 11%, and 2%, respectively [8]. Although the plant-mediated method exhibits a lower ratio compared to alternative synthesis technologies, an increasing number of researchers have focused their attention on this aspect in recent years. Li and colleagues developed an innovative method for synthesizing Fe-based samples with an average particle size of 78 nm through a reaction between eucalyptus leaf extract and $FeCl_3$ solution. These nanoparticles exhibited significant efficacy in the simultaneous removal of various antimony ions from mining solutions, with removal efficiencies of 100% and 97% for adsorption and oxidation systems, respectively [9]. In a related study, Sun et al. reported the environmentally friendly synthesis of Fe-based nanoparticles via the reaction of pomegranate leaf extract and $FeSO_4$ solution, and the particle size ranged between 75 nm and 105 nm, with a quasi-spherical morphology observed by TEM. These nanoparticles were subsequently used to degrade an indole solution, and a removal efficiency of 51.5% was achieved after 90 minutes of reaction time [10]. In addition, recent studies have explored antibacterial, antimicrobial, and antibiotic activities [11-13]. These studies highlight the considerable interest in plant-mediated synthesis of iron and iron oxide as a subject of active research in recent years. It is evident that the synthesis process using plant extracts requires a smaller amount of chemical reagents and consequently generates a lower risk of producing harmful substances. The advantage of the tea leaf synthesis process is the use of tea leaves that have been discarded after brewing, as their active ingredients, including tea polyphenols and tea pigments (theaflavins, thearubigins, and theabrownin), can still be extracted by boiling water. The waste tea leaves can be effectively reused, which further increases their practical flexibility.

Dark tea, also known as post-fermented tea, is distinguished by a unique fermentation process that differentiates it from the other six tea categories. During the process of dark tea production, microbial fermentation occurs, leading to the generation of significant amounts of tea pigments, including theabrownin, thearubigin, and theaflavin. The oxidation-reduction potential (ORP) of various dark tea infusions was evaluated to range from -63 mV to -103 mV, indicating strong antioxidant behavior [14]. From 2017 to 2023, the production of dark tea in China expanded from 28.86 to 45.8 million tons, with continued growth projected [15]. Despite this expansion, the improper disposal of dark tea residues after brewing presents a potential source of environmental pollution. In our earlier research, we elucidated the potential of tea residues as a natural sorbent for dye adsorption, with multiple adsorption-regeneration cycles successfully achieved [16, 17]. Additionally, the fabrication of nanostructured metal particles through the interaction of tea extract and a metallic precursor has been investigated. It has been determined that these particles can be used for the degradation of dyes in the Fenton-like advanced oxidation systems [18-20]. These important findings underpin the development of sustainable and reusable treatments of tea residues in environmental remediation. In contrast to the more prevalent production of green and black tea, the production of dark tea is comparatively less extensive, and its utilization in the synthesis of metal particles is less documented. The objectives of this research are to investigate the synthesis of iron particles (Fe-Ps) using dark tea extract and to identify the chemical structures of the synthesized Fe-Ps by FTIR, XRD, and XPS techniques. The catalytic activity of the synthesized Fe-Ps sample in the Fenton oxidation of malachite green (MG) was evaluated, and the reusability of the Fe-Ps was also assessed to explore their stability.

Materials and Methods

Materials

All chemicals and reagents used in the experimental procedures were of analytical grade and purchased from Sigma-Aldrich (Shanghai) Trading Co., Ltd. Ferric nitrate nonahydrate ($Fe(NO_3)_3{\cdot}9H_2O_4$) was used as an iron precursor in the synthesis process. Hydrochloric acid (HCl, 37%) and sodium hydroxide (NaOH) were used for pH adjustment of the aqueous solution. Hydrogen peroxide (H_2O_2, 30%) and malachite green (MG) were directly used in the Fenton system without further processing. Potassium bromide (KBr) was used for FTIR spectroscopy. Dark tea samples were obtained from a specialized tea market located in Fuding City, Fujian Province, China.

Synthesis of the Iron Particles

The dark tea samples were collected after brewing and subsequently washed with deionized H_2O. The washed dark tea samples were oven-dried at 50°C for 24 hours. The dried dark tea samples were crushed to pass through an 80-mesh sieve in powder form. Twenty grams of the dark tea powder were mixed with 500 mL of deionized H_2O in a reaction vessel and agitated

vigorously at 80ºC for 1 hour to extract the target compounds. After cooling, the extracted solution was centrifuged (10,000 rpm) for 5 minutes and filtered. A 0.1 mol/L of $Fe(NO_3)_3$ solution was added to the dark tea extract (volume ratio 1:3), and the mixture was stirred thoroughly on a rotary shaker for 24 hours. The resulting precipitates were isolated through centrifugation (10,000 rpm) for 5 minutes, rinsed three times with deionized H_2O, and subsequently washed twice with ethanol to ensure that the residual impurities were removed as completely as possible. After these steps, the washed samples were freeze-dried to obtain the Fe-Ps product and preserved in a thermostat for subsequent characterization and evaluation of catalytic activity.

Analytical Methods

Fourier transform infrared spectroscopy (FTIR, Thermo Scientific iS10 spectrometer) was employed to identify the functional groups and vibrational modes of the synthesized Fe-Ps in the spectral range of 4000-400 cm^{-1}. The Fe-Ps samples were homogenized with KBr at a mass ratio of 1:200, pressed into a thin disc for spectral acquisition. X-ray powder diffraction (XRD) analysis was conducted using a Bruker AXS D8 Discover with Cu Kα radiation (λ = 1.5406 Å) to determine structural properties, with diffraction patterns recorded over a 2θ range of 10° to 80°.

X-ray photoelectron spectroscopy (XPS, Thermo Scientific Nexsa G2) was performed to analyze surface elemental composition and chemical states. The wide-scan and high-resolution core-level spectra for Fe 2p and C 1s were acquired under Al Kα radiation. Measurements were performed at a pass energy of 50 eV with a 90° electron emission angle, and the binding energies of all elements were referenced to the C 1s peak at 284.6 eV.

Catalytic Experiments

The catalytic activity of the synthesized Fe-Ps sample was evaluated in a Fenton reaction system for the degradation of MG. In a typical experimental setup, the pH of the MG solution was carefully controlled at 7.0±0.2 by titration with dilute NaOH and HCl solutions. 0.1 mL of H_2O_2 was added to a reaction vessel containing 50 mL of MG solution at a concentration of 100 mg/L, followed by the addition of 50 mg of the Fe-Ps sample. The mixture was then placed in a temperature-controlled shaker and agitated at 200 rpm. After the reaction, the mixture was centrifuged at 10,000 rpm for 3 minutes to separate the solid Fe-Ps catalyst. The supernatant was collected for quantitative analysis of MG concentration using a UV-Vis spectrometer at 616 nm. Control experiments were also conducted under identical conditions without the addition of H_2O_2 to evaluate the sole adsorption efficiency.

The SPSS 16.0 software was used to evaluate statistical significance using one-way ANOVA (analysis of variance) with a 0.05 and 0.01 probability level.

Results and Discussion

Structural Characterization of the Synthesized Fe-Ps

FTIR and XRD Identification

The FTIR spectrum of the synthesized Fe-Ps is depicted in Fig. 1a). A broad band at 3418 cm^{-1} signifies the O-H stretching mode associated with hydroxyl groups. Two minor peaks at 2921 cm^{-1} and 2852 cm^{-1} correspond to the C-H stretching vibrations that are characteristic of alkane chains. A distinct split peak emerges between 2338 and 2359 cm^{-1}, which is likely attributable to fluctuations in CO_2 levels during the calibration process versus the analysis of the sample [21]. The intense band at 1648 cm^{-1} corresponds to the C=C stretching within carbonyl groups derived from tea polyphenols present in the extract [22]. A sharp peak at 1362 cm^{-1} probably relates to either C-H bending or C-N stretching vibrations. Additionally, the weaker peaks observed between 1420 cm^{-1} and 1560 cm^{-1} are associated with minor N-H bending vibrations [23]. The C-O-H stretching vibration of phenolic compounds is observed at 1027 cm^{-1}, while the C-O stretching vibration of the carbohydrate ring is noted at 1110 cm^{-1} [24, 25]. The band at 651 cm^{-1} corresponds to the iron-carbonyl complexes (Fe-C-O), thereby confirming the interaction of iron with the plant constituents [26]. The strong absorption observed below 600 cm^{-1} can be attributed to Fe-O stretching, indicating the formation of iron particles through the reaction of the iron precursor and tea extract.

The XRD pattern of the Fe-Ps sample, as illustrated in Fig. 1b), reveals a predominantly amorphous structure. The absence of sharp diffraction peaks in the XRD indicates the amorphous nature of the synthesized Fe-Ps sample. A broad hump is discernible between 38º and 45º, with a minor peak at 44º potentially corresponding to zero-valent iron (α-Fe) [27]. Moreover, a prominent hump at 23º-26º can be observed, which can be attributed to organic substances adsorbed from the dark tea leaf extract, potentially serving as a capping or stabilizing agent. Similar XRD patterns have been reported for Fe-Ps synthesized using mechanochemical activation and extracts from tobacco leaves supported by yeast [28, 29].

XPS Survey and Deconvolution of O1s and Fe 2p

The elemental binding configuration of the synthesized Fe-Ps as determined by XPS is shown in Fig. 2. The full-range scan in Fig. 2a) reveals the signals corresponding to iron (Fe), oxygen (O), nitrogen (N),

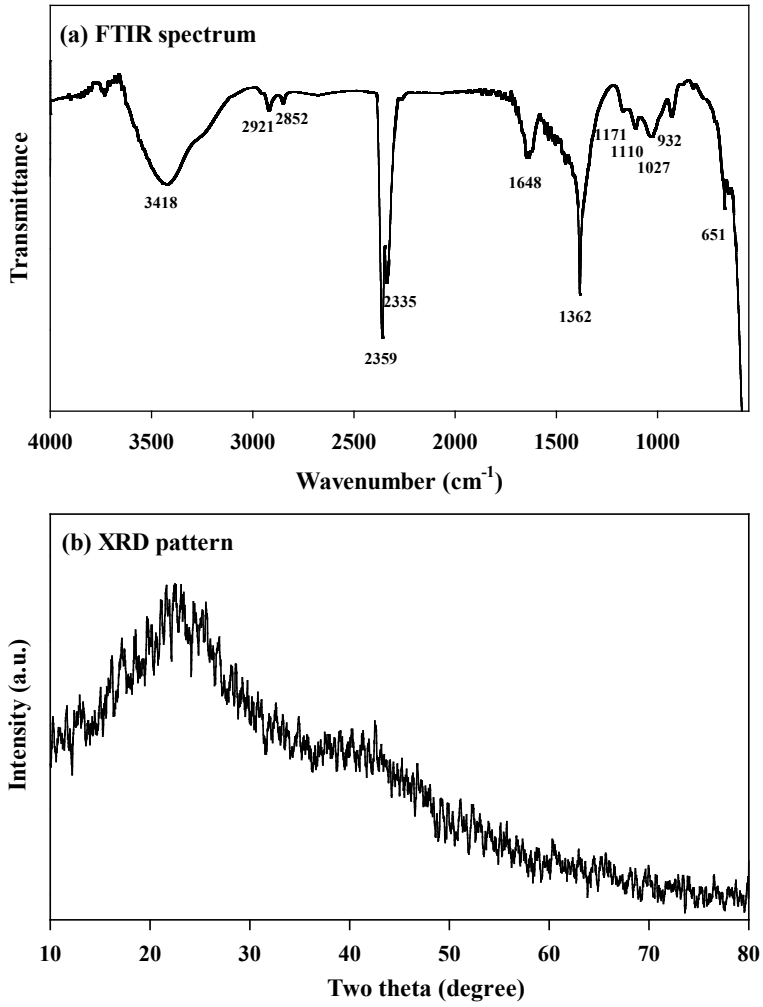

Fig. 1. a) FTIR spectrum and b) XRD pattern of the synthesized Fe-Ps.

and carbon (C) on the Fe-Ps surface. The C 1s spectrum exhibits a broad range, which was deconvoluted into three distinct regions at 284.8 eV, 286.5 eV, and 288.5 eV, respectively. The signals at 284.8 eV and 286.5 eV are assigned to C-C/C-H, C-O/C-N bonding, respectively, likely associated with the polyphenol groups bound to the Fe-Ps, and the amino acids from the dark tea extract. The higher-energy peak at 288.5 eV corresponds to functional groups such as C=O, C=N, or O-C=O. XRD analysis did not detect sharp crystalline phases, indicating the amorphous nature of the Fe-Ps sample. Consequently, deconvolution of the Fe 2p region in the XPS provides critical information regarding the valence condition. The Fe 2p region was deconvoluted to determine the iron oxidation state, revealing two prominent peaks at 711.1 eV and 724.4 eV, which correspond to the Fe 2p3/2 and Fe 2p1/2 states, respectively. In addition, the appearance of two satellite peaks is attributed to the spin-orbit split doublets of Fe 2p3/2 and Fe 2p1/2. The binding energies at 711.1 eV and 724.4 eV are indicative of Fe^{3+}, with no discernible signal or shoulder observed at lower binding energies. This observation indicates the absence of Fe^{2+} ions (~708 eV) on the surface of the sample. These energy levels suggest the presence of iron in the form of iron oxides (Fe_2O_3 or Fe_3O_4) or iron oxyhydroxide (FeOOH).

Catalytic Evaluation and Effects of Parameters on the Degradation of MG

As previously indicated, the XRD suggested the potential presence of zero-valent iron and the definitive presence of Fe^{3+} species in the sample, as determined by XPS. This is advantageous for the catalytic H_2O_2, subsequently inducing the Fenton reaction and leading to the degradation of MG. A preliminary experiment was conducted in a batch reactor for 20 minutes to assess the potential enhancement of the degradation efficiency of MG through the integrated reaction of H_2O_2 and Fe-Ps. As demonstrated in Fig. 3a), the degradation efficiencies of MG were evaluated under three different operational conditions. Conversely, the individual use of H_2O_2 and Fe-Ps showed degradation efficiencies of 6.21% and 53.48%, respectively. Notably, the degradation efficiency achieved through the Fenton reaction reached 96.93%. The ANOVA analysis further indicated

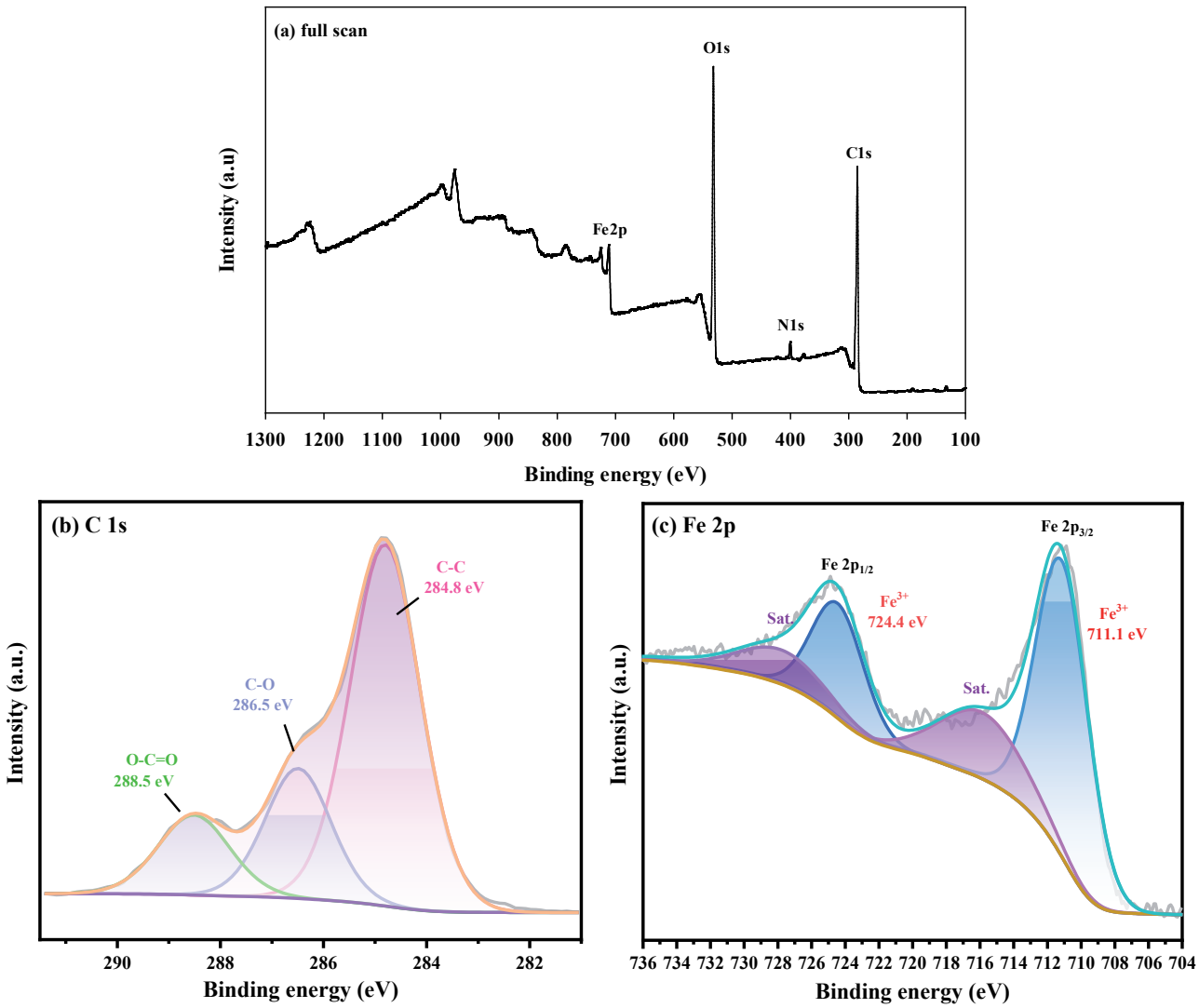

Fig. 2. XPS spectra and deconvolution analyses of the synthesized Fe-Ps: a) full scan, b) C 1s spectrum, c) Fe 2p spectrum.

a highly significant difference in the experiment ($p<0.01$). This finding suggests that the isolated use of H_2O_2 and Fe-Ps resulted in significantly lower degradation efficiencies compared to their combined application. A comprehensive evaluation of these findings reveals that Fe-Ps, acting as a catalyst within the coexistence system, facilitates the conversion of H_2O_2 into hydroxyl (OH) free radicals. These radicals subsequently react with MG, culminating in a substantial increase in degradation efficiency to 96.93%. Consequently, the Fenton system demonstrates a remarkable capability to promote MG degradation efficiency, highlighting the critical role of employing Fe-Ps in the degradation process.

A preliminary investigation was conducted to examine the impact of the Fenton reaction on the degradation efficiency of MG. A comparative experiment was conducted to provide a more comprehensive illustration of the degradation behavior of MG in the Fenton reaction. As illustrated in Fig. 3b), the Fenton reaction exerts a considerable influence compared to the individual use of H_2O_2 and Fe-Ps. The degradation efficiency rapidly exceeded 80% within 10 minutes and subsequently increased to 95% within 30 minutes. This finding suggests that the synthesized Fe-Ps catalyze H_2O_2 to generate OH free radicals as the reaction time increases. It is noteworthy that the Fe-Ps exhibited a certain degree of degradation efficiency, with a slight increase after 20 minutes, reaching approximately 55% at 180 minutes. These findings illustrate that the Fe-Ps, synthesized through the reaction of dark tea extract and an iron precursor, exhibit considerable potential for the adsorption reaction. Furthermore, the influence of the individual use of H_2O_2 on the degradation efficiency remained constant at a range of 8-10%, indicating that its effect on the degradation efficiency is not significant in this study. In summary, the application of the synthesized Fe-Ps catalyst in a Fenton system for the degradation of MG in an aqueous solution demonstrates superior degradation efficiency.

The influence of the synthesized Fe-Ps loading on the degradation efficiency of MG in a Fenton system

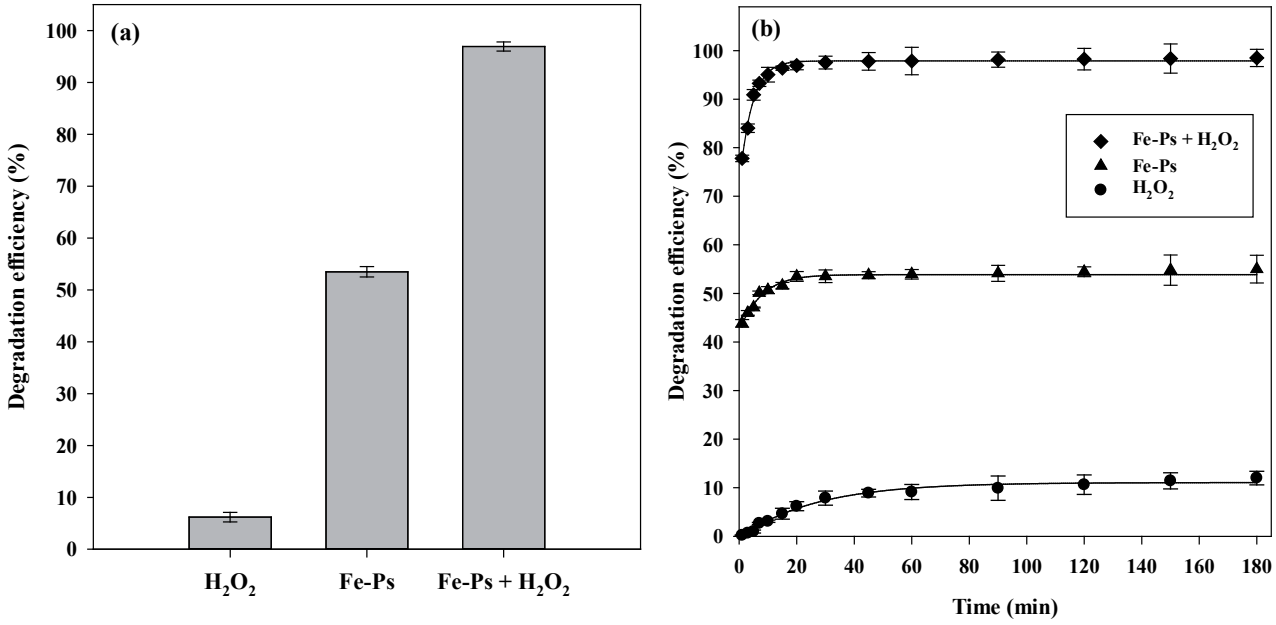

Fig. 3. Catalytic activity of the synthesized Fe-Ps for the degradation of MG in different systems: a) preliminary test ($p<0.01$) and b) effect of reaction time.

is presented in Fig. 4. A distinct improvement in degradation performance was observed, with MG degradation efficiency increasing from 27% to approximately 90% as the Fe-Ps loading increased from 10 mg to 30 mg,and a loading of 50 mg resulted in a degradation efficiency of 99.2%. A statistically significant difference between 10 and 30 mg was determined by ANOVA ($p<0.05$). This is because more Fe-Ps loading results in more OH free radical generation, which in turn results in higher degradation. In contrast, the degradation efficiency slightly decreased to 90% and 88% at 80 mg and 100 mg, respectively. No significant difference was observed within a range of 30-100 mg, as evaluated by ANOVA ($p>0.05$). This phenomenon is likely due to the presence of organic substance coatings on the Fe-Ps surface. These organic substances released from the Fe-Ps surface scavenged the OH free radicals, thereby decreasing the degradation efficiency. The feasibility of the synthesized Fe-Ps at different MG concentrations was tested. As shown in Fig. 5,

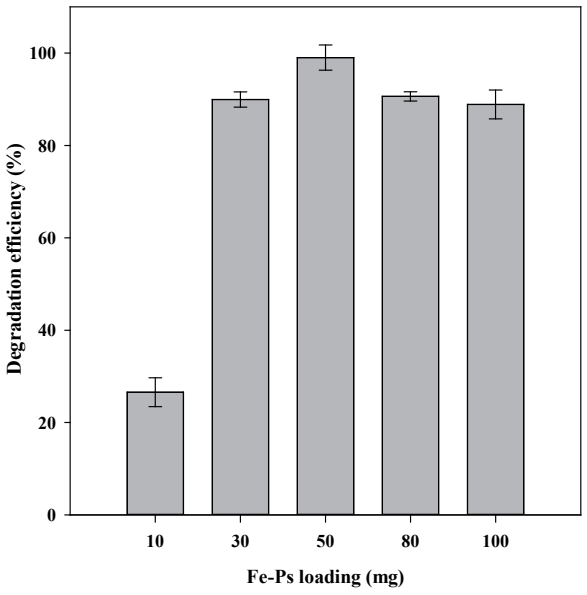

Fig. 4. Effect of Fe-Ps loading on the catalytic activity for the degradation of MG in a Fenton system ($p<0.05$ between 10-50 mg; $p>0.05$ between 30-100 mg).

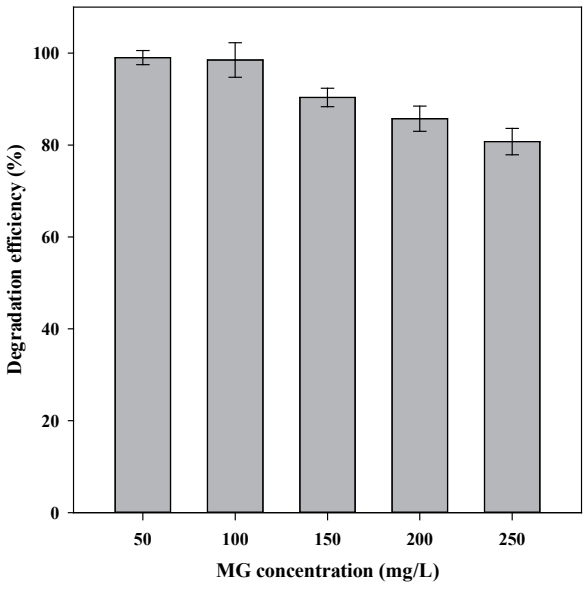

Fig. 5. Effect of MG concentration on the catalytic activity of the synthesized Fe-Ps for the degradation of MG in a Fenton system ($p<0.05$).

degradation efficiency remained above 95% within the range of 50-100 mg/L and decreased to 80% at an MG concentration of 250 mg/L. A subsequent analysis revealed a statistically significant change in degradation efficiency within the range of 50-250 mg/L ($p<0.05$). This is because the MG molecules increasingly bind to the Fe-Ps surface as the MG concentration increases. The generation of hydroxyl free radicals, on the other hand, remains constant under the given operating conditions. Under the given experimental conditions, the number of generated hydroxyl free radicals is sufficient to degrade more than 90% of the MG molecules in the range of 50-150 mg/L. To achieve 90% degradation efficiency, more hydroxyl free radicals are required when the MG concentration exceeds 200 mg/L.

Based on the experimental findings, the synthesized Fe-Ps exhibited the potential ability to degrade MG in a Fenton system. Combined with previous literature, a degradation mechanism of MG using synthesized Fe-Ps is proposed [18, 30]. Initially, MG is adsorbed onto the surface of the synthesized sample (Eq. (1)). Subsequently, the generation of hydroxyl radicals is hypothesized. The Fe^0 converts to Fe^{2+} in the presence of H_2O_2 (Eq. (2)). Then, Fe^{2+} and H_2O_2 can interact with each other to generate *OH (Eq. (3)). This process produces Fe^{3+}, which can then be reduced back to Fe^{2+} (Eq. (4)). Finally, the highly reactive *OH radicals rapidly react with the adsorbed MG, leading to the cleavage of dye molecule bonds. A portion of the MG is mineralized into CO_2 and H_2O on the surface of the synthesized Fe-Ps. The proposed degradation pathway using synthesized Fe-Ps is elucidated as follows:

Step 1: Adsorption process:

$$\mathrm{MG + Fe\text{-}Ps \rightarrow MG / Fe\text{-}Ps} \quad (1)$$

Step 2: Process of generating *OH radicals:

$$\mathrm{Fe^{o} + H_2O_2 \rightarrow Fe^{2+} + 2OH^-} \quad (2)$$

$$\mathrm{Fe^{2+} + H_2O_2 \rightarrow Fe^{3+} + OH^- + {*}OH} \quad (3)$$

$$\mathrm{Fe^{3+} + H_2O_2 \rightarrow Fe^{2+} + H^+ + {*}OOH} \quad (4)$$

Step 3: *OH radicals attack MG on the surface of Fe-Ps:

$$\mathrm{MG / Fe-Ps + {*}OH \rightarrow Reaction\ intermediates / Fe\text{-}Ps} \quad (5)$$

$$\mathrm{Reaction\ intermediates / Fe\text{-}Ps + {*}OH \rightarrow CO_2 + H_2O} \quad (6)$$

Degradation Kinetic Study

In contrast to traditional adsorption and catalytic reactions, the Fenton reaction is a complex system with over eighteen reactions that have been implicated [31-34]. The process is generally understood to involve two primary steps: rapid generation of OH through the oxidation of Fe^{2+} by H_2O_2, followed by a slower step characterized by the regeneration of ferrous [35]. The first-order and second-order kinetic models are appropriate for elucidating the initial and subsequent stages of the Fenton reaction, respectively [36, 37]. The BMG (Behnajady-Modirshahla-Ghanbary) kinetic model, originally established by Chan and Chu and subsequently modified by Behnajady and colleagues, is widely used. The BMG model effectively addresses and integrates the two primary phases of the Fenton reaction [38, 39]. The BMG kinetic model can be expressed by Eq. (7), and linearized by Eq. (8):

$$\frac{C_t}{C_o} = 1 - \left[\frac{t}{m + b \cdot t}\right] \quad (7)$$

$$\frac{t}{1 - \left(\frac{C_t}{C_o}\right)} = m + b \cdot t \quad (8)$$

Here, C_o and C_t denote the initial MG concentration and its concentration at a specific time t, respectively. Variables m (intercept) and b (slope) are fundamental constants that reflect the reaction kinetics and the degradation capacity within the BMG model. For comparison, the zero-order, first-order, and second-order kinetic models were also taken into account, as delineated by Eq. (9) to (11).

$$C_t - C_o = -k_1 t \quad (9)$$

$$\ln \frac{C_t}{C_o} = -k_2 t \quad (10)$$

$$\frac{1}{C_t} - \frac{1}{C_o} = k_3 t \quad (11)$$

The fitting results of the different kinetic models for the catalytic degradation of MG by the synthesized Fe-Ps in a Fenton system are shown in Fig. 6. The BMG model shows the most accurate fit to elucidate MG degradation kinetics in both reactions. It was observed that other models for the Fenton system exhibited a two-stage curve and a lower regression coefficient. The experimental fits are in accordance with the fundamental principles of the Fenton reaction, characterized by a rapid initial reaction phase followed by a slower subsequent reaction phase. In the BMG model, the physical significance of the 1/m represents the initial degradation rate, and the 1/m values for Fe-Ps+H_2O_2 and the individual use of H_2O_2 are 2.6008 and 0.1381, respectively. The value of 1/b can be used to evaluate the degradation capacity in the reaction. The degradation capacities of both reactions

were determined to be 0.9887 and 0.1381, respectively, indicating a more than sevenfold increase for Fe-Ps+H_2O_2 compared to the individual use of H_2O_2. The degradation capacity of Fe-Ps+H_2O_2 is consistent with the previous reports, where the values of 1/b ranged from 0.909 to 1.01 for various dyes [40, 41]. Based

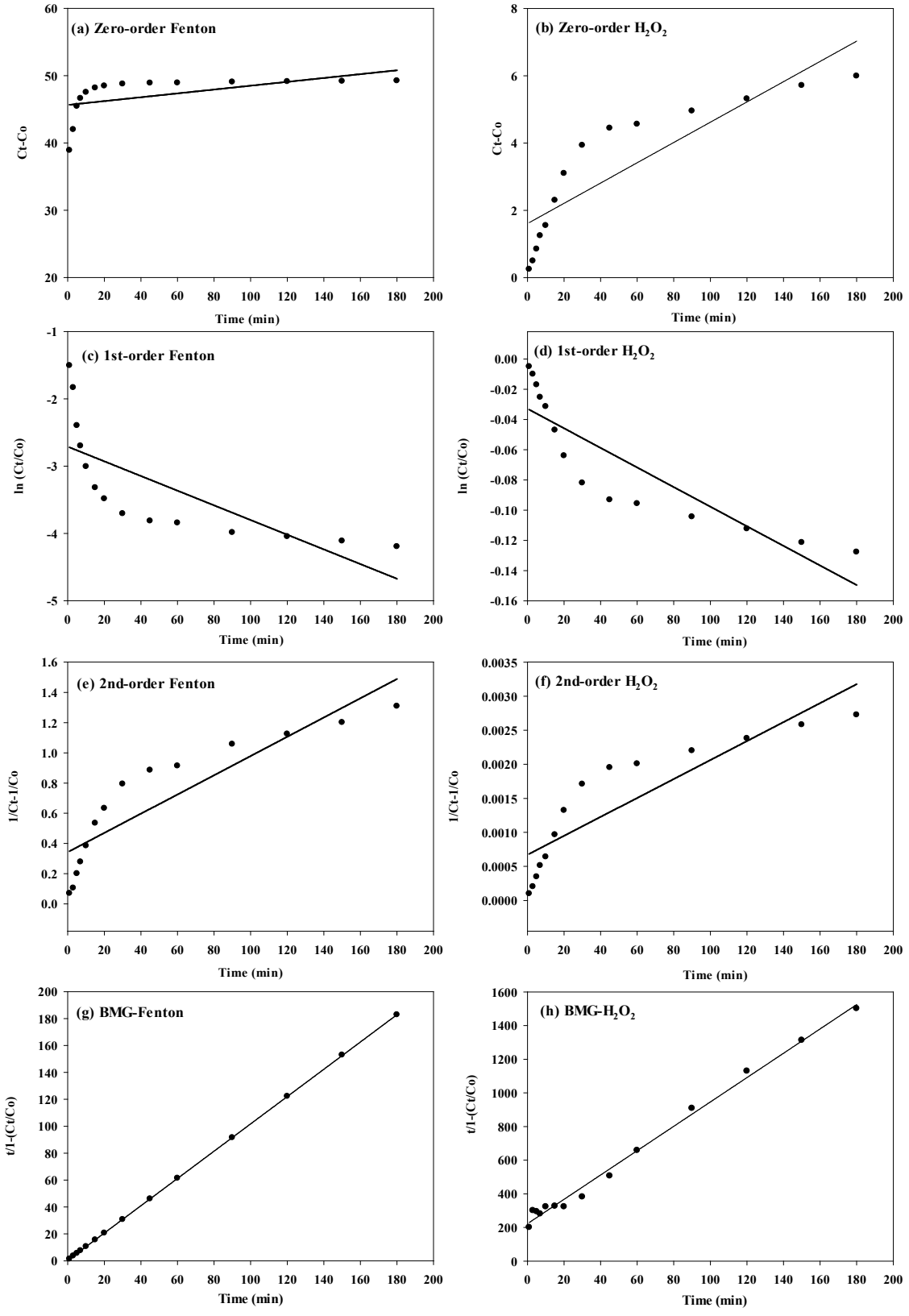

Fig. 6. Kinetic fits of the synthesized Fe-Ps for the degradation of MG: a) Zero-order of Fenton, b) Zero-order of H_2O_2, c) 1st-order of Fenton, d) 1st-order of H_2O_2, e) 2nd-order of Fenton, f) 2nd-order of H_2O_2, g) BMG of Fenton, h) BMG of H_2O_2.

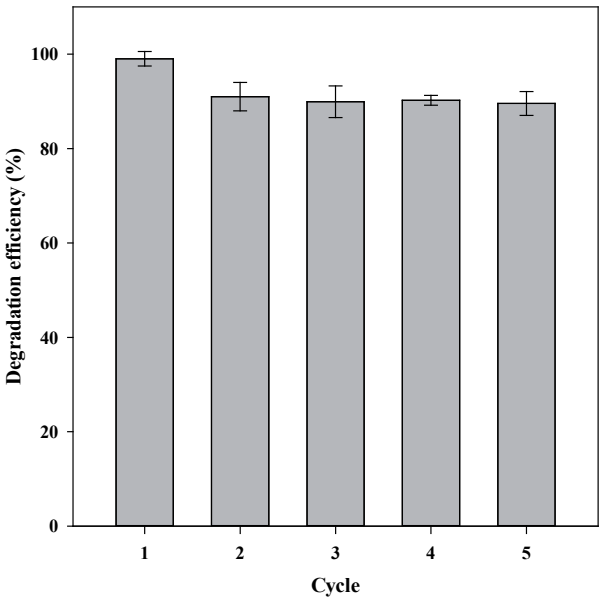

Fig. 7. Reusability of the catalytic activity of the synthesized Fe-Ps for the degradation of MG in a Fenton system ($p>0.05$ between the 2nd and 5th cycles).

on these findings, it can be concluded that the BMG kinetic model effectively characterizes the degradation of MG by the synthesized Fe-Ps. Furthermore, it has been confirmed that there is an improved degradation capacity. In fact, kinetic information can be used to evaluate the extent of pilot-scale reactions, reaction rates, and catalyst loading in real-world applications. Nevertheless, the implementation of the kinetic model necessitates consideration of several critical factors, including the effects of internal and external mass transfer and the reactor configuration (fixed-bed, fluidized-bed, or plug-flow, etc.). Moreover, despite its effective performance, the BMG model is completely empirical, and its predictions are not based on the suite of chemical reactions occurring in a Fenton process [42].

Reusability

In addition to the commendable degradation reactivity and performance of the Fe-Ps catalyst, the reusability of a catalyst is a crucial consideration from an industrial perspective. Five consecutive cycles of the synthesized Fe-Ps were evaluated. As can be seen in Fig. 7, the degradation efficiency exhibited a modest decrease from 99.82% in the first cycle to 90.22% in the fifth cycle. Statistical analysis revealed no significant variance in degradation efficiency after the first cycle ($p>0.05$). The synthesized Fe-Ps maintained reusability after the first cycle, indicating that the synthesis of Fe-Ps using tea extract is a viable and effective method for catalytic dye degradation in a Fenton system.

It is very important to understand the reason for the deactivation of the synthesized Fe-Ps. After the reusability process, the sample was characterized by XRD, N_2 adsorption, and a chloride analyzer. As shown in Fig. 8, the well-crystalline phase of the sample was observed after reusability. The main crystallite phases, hematite (α-Fe_2O_3) and goethite (α-FeOOH), have relatively lower catalytic activity compared to Fe^{2+} and Fe^0 in a Fenton system. Furthermore, the BET surface area decreased from 32.61 to 23.51 m^2/g after reusability cycles. The pore structure of the sample

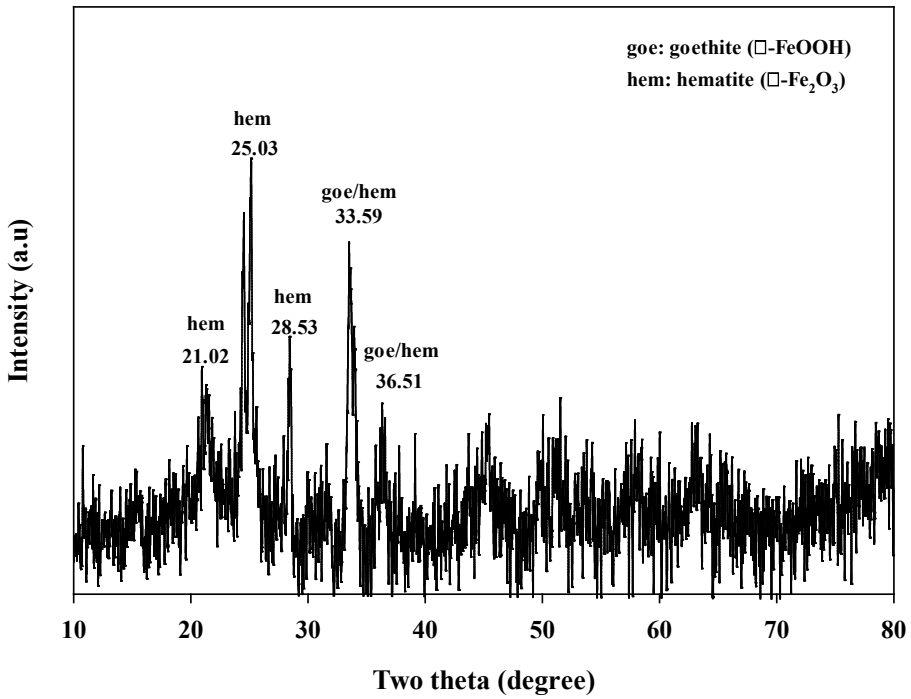

Fig. 8. XRD pattern of the synthesized Fe-Ps after five cycles.

Table 1. Comparison of green-synthesized iron particles for the catalytic degradation of dye in a Fenton system.

Raw material	Dye	Reaction time (min)	Degradation Efficiency (%)	Reference
Green tea	Malachite green	90	78.3	[43]
Tobacco leaf	Methylene blue	600	99.7	[29]
Green tea	Methylene blue Methyl orange	180	99.9 98.9	[44]
Bridelia retusa leaf	Crystal violet	270	100	[45]
Ulva spp. algae	Malachite green	240	30	[46]
Dark tea	Malachite green	120	99	This study

underwent obvious alterations. Chloride originated from the MG reagent $C_{23}H_{25}ClN_2$. The chloride content in the fresh and used samples was determined to be 4.56±0.12 mg/g and 36.23±2.02 mg/g, respectively, as determined by a chloride analyzer. This confirmed that due to the strong adsorption affinity between the sample and MG, smaller portions of the MG molecules were adsorbed onto the sample, which further reduced the catalytic activity of the sample. Overall, the observed decrease in degradation efficiency during the reusability process can be attributed to changes in the crystallite phase, the decrease in BET surface area, and the higher chloride content in the sample.

To compare the degradation ability of dye in a Fenton system using Fe-Ps synthesized from diverse plant extracts, relevant literature was collected and summarized in Table 1. The results indicate that the majority of the synthesized Fe-Ps samples exhibit efficiency in the degradation of dyes in a Fenton system. Specifically, the present study demonstrates that a degradation efficiency of 99% was achieved within 120 minutes, with more than 90% efficiency being maintained. These findings suggest that the synthesized Fe-Ps using dark tea extract are effective catalysts for H_2O_2 oxidation, facilitating MG catalytic degradation. Moreover, the use of waste dark tea is identified as a valuable biomass source.

Conclusions

The synthesis of Fe-Ps employing dark tea extracts as a reducing agent was investigated. FTIR and XRD analyses revealed the presence of polyphenols and various iron compounds, including Fe-O and Fe-O-C bonds, along with an amorphous phase. The synthesized Fe-Ps demonstrated remarkable catalytic activity in a Fenton system, achieving over 99% degradation efficiency for malachite green (MG). The optimal loading of Fe-Ps was determined to be 50 mg, with degradation efficiency exceeding 95% within the MG concentration range of 50-100 mg/L. The BMG kinetic model accurately described the degradation process, demonstrating higher reaction rate constants and degradation capacities compared to the individual use of the H_2O_2 reaction. In addition, the synthesized Fe-Ps exhibited notable reusability, maintaining consistent degradation efficiency over five consecutive cycles. In summary, the findings of this study indicate that the Fe-Ps sample synthesized through the reaction between dark tea extract and an iron precursor is a promising heterogeneous catalyst for the remediation of dye wastewater in industrial applications.

Acknowledgments

Authors acknowledge the support by the Research Projects of Ningde Normal University (2024Y12) and the Scientific Research Foundation of Ningde Normal University (2020ZX503), and Natural Science Foundation of Fujian Province (2020J05225).

Conflict of Interest

The authors declare no conflict of interest.

References

1. YAO H., HU S., WU Y., FAN L. The synergetic effects in a Fenton-like system catalyzed by nano zero-valent iron (nZVI). Polish Journal of Environmental Studies. **28** (4), 2491, **2019**.
2. ALAZBA A.A., SHAFIQ M., AMIN M.T. Transforming *Conocarpus* hedge waste into a highly effective iron/manganese nanocomposite biochar for efficient methylene blue dye removal from aqueous solution. Polish Journal of Environmental Studies. **34** (3), 3033, **2025**.
3. TACCOLA S., GRECO F., ZUCCA A., INNOCENTI, C., FERNÁNDEZ C.D.J., CAMPO G., SANGREGORIO C., MAZZOLAI B., MATTOLI V. Characterization of free-standing PEDOT: PSS/iron oxide nanoparticle composite thin films and application as conformable humidity sensors. ACS Applied Materials & Interfaces. **5** (13), 6324, **2013**.
4. RANI S.S.S., RADHIKA S., PADMA C.M. Single-domain soft ferromagnetic Sr-ZrFe composites for magnetic data storage. Ceramics International. **50** (9), 14581, **2024**.

5. TUČEK J., KEMP K.C., KIM K.S., ZBOŘIL R. Iron-oxide-supported nanocarbon in lithium-ion batteries, medical, catalytic, and environmental applications. ACS Nano. **8** (8), 7571, **2014**.
6. ALHALILI Z. Metal oxides nanoparticles: general structural description, chemical, physical, and biological synthesis methods, role in pesticides and heavy metal removal through wastewater treatment. Molecules. **28** (7), 3086, **2023**.
7. SHIMA P.D., PHILIP J., RAJ B. Synthesis of aqueous and nonaqueous iron oxide nanofluids and study of temperature dependence on thermal conductivity and viscosity. Journal of Physical Chemistry C. **114** (44), 18825, **2010**.
8. ALI A., ZAFAR H., ZIA M., UL HAQ I., PHULL A.R., ALI J.S., HUSSAIN A. Synthesis, characterization, applications, and challenges of iron oxide nanoparticles. Nanotechnology, Science and Applications. **9**, 49, **2016**.
9. LI H., GONG K., JIN X., OWENS G., CHEN Z. Mechanism for the simultaneous removal of Sb(III) and Sb(V) from mining wastewater by phytosynthesized iron nanoparticles. Chemosphere. **307** (Part 1), 135778, **2022**.
10. SUN H., LIU Y., ZHOU Y., CHEN Z., LI J. Green synthesis of iron-based nanoparticles using *Pomegranate* leaf extracts: characterization, biomolecules and indole removal. Water. **16** (18), 2665, **2024**.
11. MATAR G.H., ANDAC M. Green synthesis of iron oxide nanoparticles using brown Egyptian propolis extract for evaluation of their antibacterial activity and degradation of dyes. Inorganic Chemistry Communications. **153**, 110889, **2023**.
12. NAGARAJA K., ALMUTAIRI T.M., OH T.H. Green synthesis of iron nanoparticles using strychnos potatorum polysaccharide through *in situ* bio-reduction approach; and their antimicrobial activity. Journal of Cluster Science. **35**, 1175, **2024**.
13. RALTE L., GOSWAMI S., TIWARI D., JUNG J. Novel iron free nano-Fenton-like catalyst for sustainable treatment of antibiotics and cyanobacteria. Journal of Cleaner Production. **496**, 144982, **2025**.
14. QU X.Y., LIN S., TONG H.R. Study on relationship between main contents of polyphenols and oxidation reduction potential of Pu-er tea. Southwest China Journal of Agricultural Sciences. **27** (2), 601, **2014** [In Chinese].
15. Current analysis on dark tea industrial production in China. Available on: https://www.chinabaogao.com/detail/738050.html [in Chinese].
16. LIU X., WU Y., ZHAO W., WU Z., HAN H., XIE Z., YILMAZ M., KO T.H. Adsorption of malachite green from aqueous phase by tea stalk powder: parameters, kinetic, isothermal, and thermodynamic studies. BioResources. **18** (3), 6364, **2023**.
17. LIN D., WU F., HU Y., ZHANG T., KO T.H. Adsorption of dye by waste black tea powder: parameters, kinetic, equilibrium, and thermodynamic studies. Journal of Chemistry. **2020**, 5431046, **2020**.
18. LIU X., ZHAO W., HUANG Z., KO T.H., SONG Z., HAN H., YILMAZ M. Green synthesis of Fe-nanoparticles using pruned tea leaf extract: characterization and use for degradation of dyes from aqueous phase in Fenton-like system. Water Reuse. **14** (2), 160, **2024**.
19. HUANG F., ZHAO W., LIU X., KO T.H. Green synthesis of Cu-nanoparticles using tea stem: structural properties and application for catalytic of methylene blue. Materials Transactions. **65** (6), 707, **2024**.
20. HUANG Z., ZHAO W., LIU X., ZHONG M., YE X., KO T.H. Green synthesis of copper nanoparticles using white tea leaf extract: characterization, catalytic and antibacterial applications. BioResources. **19** (3), 5031, **2024**.
21. TARASCHEWSKI M., CAMMENGA H.K., TUCKERMANN R., BAUERECKER S. FTIR study of CO_2 and H_2O/CO_2 nanoparticles and their temporal evolution at 80 K. Journal of Physical Chemistry A. **109** (15), 3337, **2005**.
22. DAS R.K., BORTHAKUR B.B., BORA U., Green synthesis of gold nanoparticles using ethanolic leaf extract of *Centella asiatica*. Materials Letters. **64** (13), 1445, **2010**.
23. CHATTERLEY A.S., LAITY P., HOLLAND C., WEIDNER T., WOUTERSEN S., GIUBERTONI G. Broadband multidimensional spectroscopy identifies the amide II vibrations in silkworm films. Molecules. **27** (19), 6275, **2022**.
24. JAYEOYE T.J., EZE F.N., OLATUNJI O.J., TYOPINE A.A. Synthesis of biocompatible Konjac glucomannan stabilized silver nanoparticles, with *Asystasia gangetica* phenolic extract for colorimetric detection of mercury (II) ion. Scientific Reports. **12**, 9176, **2022**.
25. HAMZA M.F., FOUDA A., WEI Y., EL AASSY I.E., ALOTAIBI S.H., GUIBAL E., MASHAAL N.M. Functionalized bio-based composite for metal decontamination-insight on uranium and application to water samples collected from wells in mining areas (Sinai, Egypt). Chemical Engineering Journal. **431** (1), 133967, **2022**.
26. MADIVOLI E.S., KARERU P.G., GACHANJA A.N., MUGO S.M., MAKHANU D.S. Phytofabrication of iron nanoparticles and their catalytic activity. SN Applied Sciences. **1**, 879, **2019**.
27. MA D., LI X., ZOU H., QIAN Y., LI M., XU W. Enhanced nitrate reduction by HPMC-stabilized nanoscale zero-valent iron (H-NZVI): synthesis, characterization and reaction kinetics. Desalination and Water Treatment. **322**, 101164, **2025**.
28. MOLLA A., CHOI H., YOUK J.H. Mechanochemical activation of zero-valent iron on carbonized boron-doped graphene dots for enhanced sonochemical dyes removal. Colloid and Interface Science Communications. **45**, 100548, **2021**.
29. SHI G., ZENG S., LIU Y., XIANG J., DENG D., WU C., TENG Q., YANG H. Efficient heterogeneous Fenton-like degradation of methylene blue using green synthesized yeast supported iron nanoparticles. Ecotoxicology and Environmental Safety. **263**, 115240, **2023**.
30. BERGENDAHLA J.A., THIES T.P. Fenton's oxidation of MTBE with zero-valent iron. Water Research. **38** (2), 327, **2004**.
31. LI Y., CHENG H. Chemical kinetic modeling of organic pollutant degradation in Fenton and solar photo-Fenton processes. Journal of Taiwan Institute of Chemical Engineers. **123**, 175, **2021**.
32. BEHROUZEH M., ABBASI M., OSFOURI S., DIANAT M.J. Treatment of DMSO and DMAC wastewaters of various industries by employing Fenton process: process performance and kinetics study. Journal of Environmental Chemical Engineering. **8** (1), 103597, **2020**.
33. ENAMI S., SAKAMOTO Y., COLUSSI A.J. Fenton chemistry at aqueous interfaces. PNAS. **111** (2), 623, **2014**.
34. KUMAR J.E., MULAI T., TRIPATHY A. Behnajady-Modirshahla-Ghanbary kinetic models for degradation of azo dye using Fenton oxidation process: a mini review. Next Research. **1** (2), 100047, **2024**.
35. SHARMA A., VERMA M., HARITASH A.K. Degradation of toxic azo dye (AO7) using Fenton's

process. Advances in Environmental Research. **5** (3), 189, **2016**.
36. LI A., FANG X., SUN J., LIU Q., LIAN Y., LI S., AN Y., WANG Y., GAO A. Analyzing the kinetics of degradation of acid red B dye through Fenton oxidation with online monitoring system. Desalination and Water Treatment. **216**, 412, **2021**.
37. BAHMANI P., MALEKI A., GHAHRAMANI E., RASHIDI A. Decolorization of the dye reactive black 5 using Fenton oxidation. African Journal of Biotechnology. **12** (26), 4115, **2013**.
38. CHAN K.H., CHU W. Modeling the reaction kinetics of Fenton's process on the removal of atrazine. Chemosphere. **51** (4), 305, **2003**.
39. BEHNAJADY M.A., MODIRSHAHLA N., GHANBARY F. A kinetic model for the decolorization of C.I. acid yellow 23 by Fenton process. Journal of Hazardous Materials. **148** (1-2), 98, **2007**.
40. PANIĆ S., PETRONIJEVIĆ M., VUKMIROVIĆ J., GRBA N., SAVIĆ S. Green synthesis of nanoscale zero-valent iron aggregates for catalytic degradation of textile dyes. Catalysis Letters. **153**, 3605, **2023**.
41. MENG G., LIU B., SUN M., MIAO Q., DING S., ZHANG J., LIU Z. Sludge-based activated carbon catalyzed H_2O_2 oxidation of reactive azo dyes. Environmental Technology. **42** (5), 682, **2021**.
42. LI Y., CHENG H. Chemical kinetic modeling of organic pollutant degradation in Fenton and solar photo-Fenton processes. Journal of the Taiwan Institute of Chemical Engineers. **123**, 175, **2021**.
43. WU Y., ZENG S., WANG F., MEGHARAJ M., NAIDU R., CHEN Z. Heterogeneous Fenton-like oxidation of malachite green by iron-based nanoparticles synthesized by tea extract as a catalyst. Separation and Purification Technology. **154**, 161, **2015**.
44. SHAHWAN T., SIRRIAH S.A., NAIRAT M., BOYACI E., EROGLU A.E., SCOTT T.B., HALLAM K.R. Green synthesis of iron nanoparticles and their application as a Fenton-like catalyst for the degradation of aqueous cationic and anionic dyes. Chemical Engineering Journal. **172**, 258, **2011**.
45. SELVARAJ R., PAI S., MURUGESAN G., PANDEY S., BHOLE R., GONSALVES D., VARADAVENKATESAN T., VINAYAGAM R. Green synthesis of magnetic α-Fe_2O_3 nanospheres using *Bridelia retusa* leaf extract for Fenton-like degradation of crystal violet dye. Applied Nanoscience. **11** (1), 1, **2021**.
46. ERGÜT M., UZUNOĞLU D., ÖZER A. Efficient decolourization of malachite green with biosynthesized iron oxide nanoparticles loaded carbonated hydroxyapatite as a reusable heterogeneous Fenton-like catalyst. Journal of Environmental Science and Health, Part A. **54** (8), 786, **2019**.